Proceedings of ERAD 2006

Quantification of uncertainties in attenuation correction for single-polarization weather radars at C- and X-band

Alexis Berne[1], **Remko Uijlenhoet**[2], **Gianfranco Vulpiani**[3], **and Frank Marzano**[4,5]

[1]Laboratoire d'étude des Transferts en Hydrologie et Environnement, Grenoble (France).
[2]Hydrology and Quantitative Water Management Group, Wageningen University (The Netherlands).
[3]Météo France, Trappes (France).
[4]University of L'Aquila, CETEMPS (Italy).
[5]University La Sapienza of Rome, Dept. of Electronic Eng. (Italy).

1 Introduction

At C- or X-band wavelengths, the importance of attenuation affecting the radar signal in rain has been recognized for a long time. Because of the non-sphericity of rain drops, backscaterring and propagation of electromagnetic waves depend on their polarization state. As most operational weather radars in Europe are single-polarization C-band systems, the quantification of the influence of uncertainties concerning (1) radar calibration, (2) the parameterization of power law relations between the integral variables (in particular radar reflectivity Z and specific attenuation k), and (3) total path integrated attenuation (PIA) estimates, at the horizontal and vertical polarization states, is highly relevant. In this work, we focus on two attenuation correction algorithms: a forward (Hitschfeld and Bordan, 1954) and a backward (Marzoug and Amayenc, 1994) scheme.

A stochastic simulator of range profiles of raindrop size distributions (DSD) is used to generate 1000 DSD profiles of 50 km, from which the corresponding radar variables (i.e., reflectivity Z, specific attenuation k and rain rate R) are derived for the horizontal and vertical polarization states (H and V in the following) of the radar signal, using a T-matrix code (Vulpiani et al., 2006). Within this controlled experiment framework, the influence of the three sources of error previously mentioned is quantitatively investigated.

The paper is organized as follows: the DSD simulator is briefly described in Section 2; Section 3 presents the attenuation correction algorithms; the sensitivity analysis is presented in Section 4 and the performance of the two algorithms for the two polarization states is compared in Section 5.

Correspondence to: Alexis Berne
(Alexis.Berne@hmg.inpg.fr)

2 DSD simulator

The range profiles of DSDs have been generated using a modified version of the stochastic simulator proposed by Berne and Uijlenhoet (2005). It is based on an gamma DSD model with a fixed shape parameter ($\mu = 3$):

$$N(D_e|N_t,\Lambda) = N_t \frac{\Lambda^4}{\Gamma(4)} D_e^3 e^{-\Lambda D_e} , \qquad (1)$$

where $N(D_e|N_t,\Lambda)dD_e$ denotes the drop concentration in the equivolumetric spherical diameter interval $[D_e, D_e + dD_e]$ given N_t (drop concentration in m^{-3}) and Λ (in mm^{-1}). The two parameters N_t and Λ are assumed to be random variables, jointly lognormally distributed. To introduce a spatial structure in the profiles, $N' = \ln N_t$ and $\Lambda' = \ln \Lambda$ are assumed to follow a first order discrete vector auto-regressive process. This results in an exponential autocorrelation function:

$$\rho(r) = e^{-2r/\theta} , \qquad (2)$$

where r represents the distance lag and θ the characteristic spatial scale, also known as the scale of fluctuation. The stochastic simulator is used to produce 1000 range profiles of DSDs of equivolumetric spherical drops. Using a similar approach to that used in Vulpiani et al. (2006), the corresponding profiles of co-polarized radar reflectivity factor Z and specific attenuation k at H and V polarization states are derived.

DSD time series measurements from an optical spectropluviometer, collected on 7 September 1998, during the HIRE'98 experiment in Marseille, France, are used to parameterize the simulator. Assuming Taylor's hypothesis with a constant velocity of 12.5 m s^{-1}, the required spatial characteristics of N' and Λ' are derived. To achieve a spatial resolution of 50 m, DSD data have been analyzed at a 4-s time step. The length of the profiles is fixed to 50 km. The

Table 1. Mean, standard deviation and characteristic spatial scale of $N' = \ln N_t$ and $\Lambda' = \ln \Lambda$ deduced from HIRE'98 data (07/09/1998 event) at a 4-s time step.

	Mean	Std	θ (km)
N'	6.29	0.43	6.25
Λ'	1.56	0.19	6.25

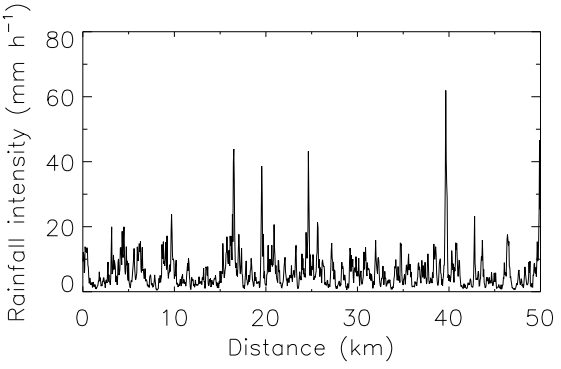

Fig. 1. Example of generated profile of rain rate R.

analysis of the fitted N' and Λ' values shows that their cross-correlation can be considered as negligible. The number of model parameters now reduces to five: the mean and standard deviation of N' and Λ', and the characteristic scale θ (assumed to be equal for N' and Λ'). Their values are given in Table 1.

Fig. 1 presents an example of generated profile of rain rate R. This controlled experiment framework allows to adopt a Monte Carlo approach to quantitatively investigate the influence of uncertainties concerning radar calibration, parameterization of the Z-k power-law relation, and PIA estimates for H and V polarizations.

3 Attenuation correction algorithms

Two different types of algorithms will be studied in the following. The first attenuation correction algorithm corresponds to a forward implementation and is based on the analytical solution proposed by Hitschfeld and Bordan (1954). The second algorithm corresponds to a backward implementation and is based on the analytical solution proposed by Marzoug and Amayenc (1994). The following equations are valid for both horizontal and vertical polarization states.

The measured attenuated reflectivity Z_a reads

$$Z_a(r) = \delta_c A(r) Z(r) \ , \tag{3}$$

where δ_c is the calibration error factor and $A(r)$ is the two-way attenuation factor at the range r ($0 \leq A \leq 1$). Assuming the Z-k relation reads

$$Z = \delta_\alpha \alpha \, k^{\delta_\beta \beta} \ , \tag{4}$$

where δ_α (δ_β respectively) is the error factor in α (β), A can be written as

$$A(r) = \exp\left[-0.2\ln(10)\int_0^r \left(\frac{Z(s)}{\delta_\alpha \alpha}\right)^{1/(\delta_\beta\beta)} ds\right] \ . \tag{5}$$

Hitschfeld and Bordan (1954) (HB hereafter) proposed an analytical solution to express Z as a function of Z_a:

$$Z(r) = Z_a(r) \Big/ \left[\delta_c^{1/(\delta_\beta\beta)} - \frac{0.2\ln(10)}{\delta_\beta\beta}\int_0^r \left(\frac{Z_a(s)}{\delta_\alpha\alpha}\right)^{1/(\delta_\beta\beta)} ds\right]^{\delta_\beta\beta} \ . \tag{6}$$

The HB algorithm is a forward algorithm because the integral is between 0 and r. However, the difference in its denominator can be close to 0 and this makes the algorithm potentially highly unstable (Hitschfeld and Bordan, 1954).

To avoid instability problems, another family of attenuation correction algorithms has been developed. It is based on the knowledge of an estimate A_0 of the PIA at a given range r_0. For ground-based radar, ground echoes may be used to derive PIA estimates by comparing their reflectivity values during dry and rainy periods, as proposed by Delrieu et al. (1997). The estimate A_0 can be uncertain, that is

$$A(r_0) = \delta_A A_0 \ , \tag{7}$$

where δ_A is the error factor in A_0. The reformulation of Eq.(6) starting from r_0 and going backward to the radar guarantees the stability of the algorithms. As an example, we use the solution proposed by Marzoug and Amayenc (1994) (MA hereafter):

$$Z(r) = Z_a(r) \Big/ \left[(\delta_c\delta_A A_0)^{1/(\delta_\beta\beta)} + \frac{0.2\ln(10)}{\delta_\beta\beta}\int_r^{r_0} \left(\frac{Z_a(s)}{\delta_\alpha\alpha}\right)^{1/(\delta_\beta\beta)} ds\right]^{\delta_\beta\beta} \ . \tag{8}$$

The main drawback of such a backward algorithm is that it requires a reliable estimation of the PIA at a given range.

4 Sensitivity analysis

To study the sensitivity of the two algorithms to the different sources of error mentioned in the introduction, we use a Monte Carlo technique. One thousand profiles of N_t and Λ (hence of Z, k and Z_a) are generated for H and V polarizations. On each profile a Z-k power-law relation is fitted by means of a non-linear regression technique. The exact

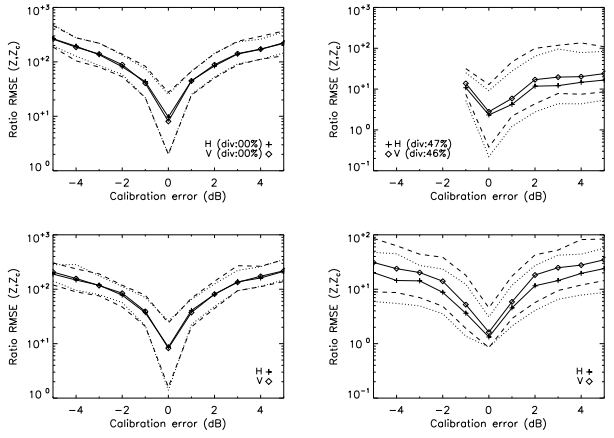

Fig. 2. Median, 10% and 90% quantiles of the distribution of the RMSE ratio as a function of the calibration error ϵ_c expressed in dB, for H and V polarizations, for the HB (top panels) and the MA (bottom panels) algorithms. The left panels correspond to C-band (5.6 cm) and the right panels to X-band (3.2 cm).

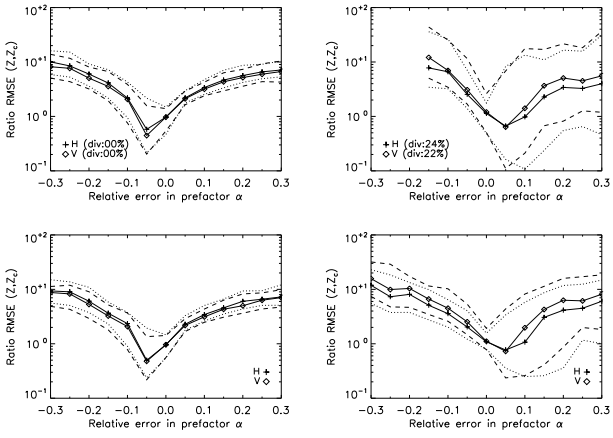

Fig. 3. Same as Figure 2, but the relative error in the prefactor α of the relation $Z = \alpha k^{\beta}$.

PIA value is calculated as the difference between the non-attenuated and the attenuated Z profiles. Then the two algorithms are applied using the fitted relations on the 1000 profiles. This procedure is applied for both H and V polarizations. Using these reference values enables to independently analyze the influence of the different sources of error on the two attenuation correction algorithms.

4.1 Influence of the uncertainty in calibration

Radar systems can be affected by calibration errors. In this section, the influence of the uncertainty in calibration on the accuracy of the attenuation correction algorithms is quantified. For better visual inspection, the calibration error is expressed in dB as $\epsilon_c = 10\ \log_{10}(\delta_c)$ and varies in the interval [-5,+5]. The additional error due to uncertain calibration is calculated as the ratio between the RMSE values for a given calibration error and the reference (for $\delta_c = 1$) RMSE values, for both H and V polarizations. Figure 2 presents the median, as well as the 10% and 90% quantiles, of the distribution of the RMSE ratio as a function of the calibration error for both algorithms at C- and X-band. The other error factors (δ_α, δ_β and δ_A) are fixed to 1.

The uncertainty in calibration has a strong influence on the accuracy of the two attenuation algorithms, and the RMSE ratio is larger at C-band than at X-band. For instance, when $\epsilon_c = +1$ dB, the RMSE ratio is about 35 at C-band while it is about 5 at X-band for both algorithms. Moreover, the influence of calibration error is similar for the H and V polarizations at C-band, while it is slightly larger for V polarization at X-band. The HB algorithm is also more sensitive to underestimation ($\epsilon_c < 0$) and becomes unstable when $\epsilon_c < -1$ (absence of points in the top right panel of Fig. 2). It must be noted that the quantiles of the RMSE ratio are not exactly equal to 1 when $\epsilon_c = 0$ because the calculations are performed on 1-dB wide classes of ϵ_c.

4.2 Influence of the uncertainty in the parameterization of the *Z-k* relation

To analyze the influence of the uncertainty in the parameters of the Z-k power law on the accuracy of the two attenuation correction algorithms, an error factor between 0.7 and 1.3 is applied to the prefactor and the exponent. The additional error due to uncertain parameterization of the Z-k relation is calculated as the ratio between the RMSE values for a given prefactor (exponent) error and the reference RMSE values, for both H and V polarizations. Figures 3 and 4 present the median, as well as the 10% and 90% quantiles, of the distribution of the RMSE ratio as a function of the relative error in the prefactor and exponent, with respect to the reference Z-k relation, for both algorithms at C- and X-band. The other error factors (δ_c and δ_A) are fixed to 1.

The two algorithms have a similar sensitivity to the uncertainty in the prefactor α and the exponent β, in particular at C-band. Concerning the prefactor, the error due to attenuation correction can be partially compensated (RMSE ratio $<$ 1) when α is slightly underestimated at C-band, or conversly when α is slightly overestimated at X-band. Moreover, the dispersion is larger when α is overestimated at X-band, for both algorithms. Concerning the exponent, the compensation is less significant (only the 10% quantiles indicate it. Both algorithms are more sensitive to uncertainties in the exponent than in the prefactor. The HB algorithm is more divergent when the exponent is overestimated.

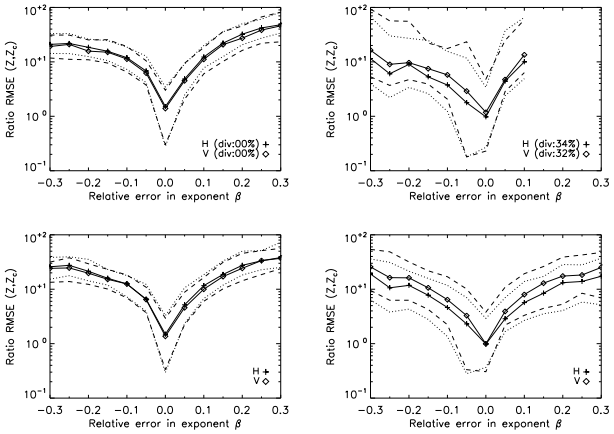

Fig. 4. Same as Figure 3, but the relative error in the exponent β of the relation $Z = \alpha k^{\beta}$.

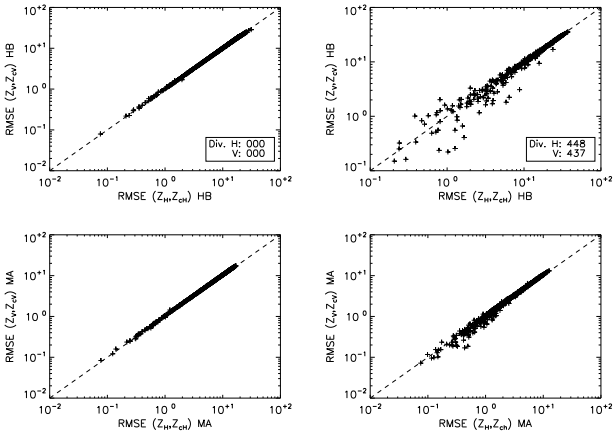

Fig. 5. Scatter diagram of RMSE (normalized by the mean Z value along the profile) for a radar system with uncertain calibration and for H and V polarizations at C- (left panels) and X-band (right panels).

4.3 Influence of the uncertainty in the PIA estimate

The MA algorithm is more accurate and more robust than the HB algorithm, but it requires an additional parameter which is the estimate of the PIA at a given range. Equation (8) shows that the influence of δ_A is the same as the influence of δ_c. Therefore, if we define $\epsilon_A = 10\,\log(\delta_A)$, the bottom panels of Fig. 2 can be used to quantify the influence of the uncertainty in PIA estimates, by interchanging ϵ_c and ϵ_A.

5 Performance comparison

From the previous section, it appears that the sensitivity of the HB and MA algorithms to the uncertainty in radar calibration, in the parameterization of the Z-k relation and in the PIA estimates (for the MA algorithm) is similar for H and V polarizations at C-band, but stronger for V polarization at X-band. At this stage, it is necessary to directly compare the overall performance of the two algorithms for the two polarization states.

As an example, Fig. 5 presents the scatter plots of RMSE values (normalized by the mean Z value along the profile to avoid bias due to higher Z values at H than at V polarizations) corresponding to a radar system with an uncertain calibration. Figure 5 shows that, for the two attenuation correction algorithms tested in this work, there is no significant difference between H and V polarization at C-band, while there is a limited increase of RMSE for H polarization, with respect to V polarization, at X-band. For lack of space, the scatter diagrams similar to those in Fig. 5 for the other studied sources of uncertainty are not displayed, but the general behaviour remains the same.

Therefore, regarding attenuation correction for single-polarization radar systems, there is no clear advantage to prefer one polarization state over another at C-band (like most European operational radar systems), while it is preferable to choose the vertical polarization state at X-band.

Acknowledgements. The first two authors acknowledge financial support from EU project FLOODsite (GOCE-CT-2004-505420). The second and third authors are also supported by the Netherlands Organization for Scientific Research (NWO, grant 016.021.003, *Vernieuwingsimpuls*).

References

Berne, A. and Uijlenhoet, R.: A stochastic model of range profiles of raindrop size distributions: application to radar attenuation correction, Geophys. Res. Lett., 32, L10803, doi:10.1029/2004GL021899, 2005.

Delrieu, G., Caoudal, S., and Creutin, J.-D.: Feasibility of using mountain return for the correction of ground-based X-band weather radar data, J. Atmos. Oceanic Technol., 14, 368–385, 1997.

Hitschfeld, W. and Bordan, J.: Errors inherent in the radar measurement of rainfall at attenuating wavelengths, J. Meteor., 11, 58–67, 1954.

Marzoug, M. and Amayenc, P.: A class of single- and dual-frequency algorithms for rain-rate profiling from a spaceborne radar. Part I: principle and tests from numerical simulations, J. Atmos. Oceanic Technol., 11, 1480–1506, 1994.

Vulpiani, G., Marzano, F., Chandrasekar, V., Berne, A., and Uijlenhoet, R.: Rainfall rate retrieval in presence of path attenuation using C-band polarimetric weather radars, Nat. Hazard. Earth Sys. Sci., 6, 439–450, 2006.